Science Bulletin 64 (2019) 158–165

Contents lists available at ScienceDirect

Science Bulletin

journal homepage: www.elsevier.com/locate/scib

Article

Co_9S_8 nanowires@NiCo LDH nanosheets arrays on nickel foams towards efficient overall water splitting

Jingan Yan, Ligang Chen, Xin Liang *

State Key Laboratory of Chemical Resource Engineering, and Beijing Key Laboratory of Energy Environmental Catalysis, Beijing University of Chemical Technology, Beijing 100029, China

ARTICLE INFO

Article history:
Received 7 November 2018
Received in revised form 10 December 2018
Accepted 20 December 2018
Available online 9 January 2019

Keywords:
Co_9S_8 nanowire
NiCo LDH
Hydrogen evolution reaction
Oxygen evolution reaction
Water splitting

ABSTRACT

Water electrolysis is considered to be an effective way to fabricate hydrogen, and it is desirable to find the highly efficient, inexpensive and good durability bifunctional electrocatalysts for overall water splitting. In this paper, we synthesis a unique structured catalyst that was composed by Co_9S_8 nanowires and nickel cobalt layered double hydroxide (NiCo-LDH) nanosheets. The ultrathin nanosheets decorated on the Co_9S_8 nanoarrays offer large specific surface area, numerous active edge sites and excellent electrical conductivity for fast electron transfer. Benefiting from this heterogeneous structure, the catalyst presents excellent catalytic performance in alkaline media. It requires 168 mV to reach current density of 10 mA/cm^2 for HER and 278 mV to reach current density of 30 mA/cm^2 for OER. When used as electrode in a homemade two-electrode system, it only needs t a voltage of 1.63 V to achieve current densities of 10 mA/cm^2, which proves Co_9S_8@NiCo LDH/NF as a superior bifunctional catalyst for water splitting.

1. Introduction

Hydrogen is highly competitive among numerous energy sources for its clean, high abundance and high energy density [1,2]. Electrolytic water splitting is an effective and clean way to fabricate hydrogen. It contains two half reactions: hydrogen evolution reaction (HER) happens on cathode side and oxygen evolution reaction (OER) happens on anode side [3,4]. Pt is the best HER performance [5], and RuO_2 and IrO_2 are the most efficient OER catalysts. But they cannot achieve large-scale applications because of their high costs and scarcities [6,7]. Thus, it is desirable to find low cost electrocatalysts which are catalytically active for both HER and OER.

Over the past few years, researchers have put a lot of efforts into finding the bifunctional electrocatalysts for OER and HER and made great progress. Non-precious metal based catalysts, including metal hydroxides [8,9], oxides [10,11], phosphides [12,13], sulfides [14,15] and selenides [16,17], have gained considerable attention. However, the performance of non-noble metal electrocatalysts is still lower than that of noble metal catalysts, and most of them are catalytically active for single reaction. The composite of two or three kinds of non-precious components is an effective approach to enhance the electrocatalytic activity by synergistic effect, and to develop bifunctional catalysts. Nanoarray architectures grown on Ni foam (NF) show excellent electrolytic water performance for their large surface areas, strong conductivity, high stability and efficient electron transfer [18–21]. For example, $NiCo_2P_x$@CoNi$(OOH)_x$ arrays on NF shows excellent OER performance [22]. $NiCoSe_2$ nanobrush arrays on NF can afford current density of 10 mA/cm^2 at overpotential of 274 mV in alkaline media towards OER [23]. Thus, the rational design on the chemical compositions and structures of the nanoarrays brings opportunities for the development of electrolytic water catalysts.

Herein, we report the three-dimensional (3D) hierarchical core-shell structure of Co_9S_8@NiCo-LDH on NF. NF was served as the electrode substrates because of its 3D porous structure and superior electrical conductivity. The NiCo-LDH ultrathin nanosheets grown on Co_9S_8 nanowires provide a lot of exposed active sites. This unique nanoarchitecture ensures efficient electron, mass transfer and intimate contact with the electrolyte. Consequently, the 3D core-shell nanostructure displays excellent OER and HER performance in alkaline media (1 mol/L KOH). It requires 168 mV to achieve 10 mA/cm^2 for HER and 278 mV to achieve 30 mA/cm^2 for OER. Simultaneously, Co_9S_8@NiCo-LDH has lower tafel slope, smaller charge transfer resistance and larger electrochemically active surface area compare with Co_9S_8/NF and NiCo LDH/NF. When used for overall water splitting, it only needs 1.63 V to reach a current density of 10 mA/cm^2.

* Corresponding author.
E-mail address: liangxin@mail.buct.edu.cn (X. Liang).

https://doi.org/10.1016/j.scib.2019.01.006
2095-9273/

2. Experimental

2.1. Chemicals and materials

NF with a thickness of 1 mm was purchased from Shanxi Liziyuan Co., Ltd. Nickel nitrate hexahydrate ($Ni(NO_3)_2{\cdot}6H_2O$), cobalt nitrate hexahydrate ($Co(NO_3)_2{\cdot}6H_2O$), urea ($CO(NH_2)_2$), poly(vinylpyrrolidone) (PVP, M_w = 30,000), ammonium fluoride (NH_4F), sodium sulfide hydrates ($Na_2S{\cdot}9H_2O$) were bought from Sinopharm Chemical Reagent Co., Ltd. All chemical reagents were of analytical grade and used as received.

2.2. Synthesis of Co_9S_8 nanowires on NF

Co_9S_8 nanoarrays on NF was prepared by a two-step hydrothermal reaction. Before synthesis, the NF (2 cm × 3 cm) was ultrasonically with 3 mol/L HCl and acetone for 15 min in sequence, next, washed thoroughly with deionized water and ethanol, and dried in vacuum at 60 °C. In a typical synthesis, 1.5 mmol $Co(NO_3)_2{\cdot}6H_2O$, 1.5 mmol NH_4F, 7.5 mmol urea were dissolved in 30 mL deionized water and stirred vigorously to obtain transparent solution, then a piece of NF was immersed into a Teflon-lined stainless-steel autoclave containing above solution. Then sealed autoclave and put it into an oven at 120 °C for 6 h. After cooling down, the NF was taken out and ultrasonic in ethanol and deionized water, followed by drying at 60 °C. Next, the NF was immersed in 30 mL 0.1 mol/L Na_2S solution, then kept at 120 °C for 6 h in an oven. When the reaction was finished, the NF was ultrasonically with ethanol and deionized water again to remove residual ingredients. Finally, the NF was dried at 60 °C in an oven.

2.3. Synthesis of Co_9S_8@NiCo-LDH on NF

To fabricate NiCo-LDH nanosheets on Co_9S_8 nanoarrays, 100 mg $Ni(NO_3)_2{\cdot}6H_2O$, 100 mg $Co(NO_3)_2{\cdot}6H_2O$, 200 mg urea, 50 mg PVP were dissolved in 15 mL ethanol and 15 mL deionized water. After stirring, the solution was poured in a 50 mL autoclave, then the above obtained Co_9S_8/NF were immersed into it and kept at 90 °C for 10 h. when the reaction was over, taken out the NF and rinsed with deionized water and ethanol, finally, dried at 60 °C.

2.4. Characterizations

The power X-ray diffraction (XRD) patterns were recorded with a Bruker D8 diffractometer using Cu Kα as the radiation source. Scanning electron microscope (SEM) with a Hitachi S4700 operates at 20 kV and transmission electron microscopy (TEM) with a FEI Tecnai G220 operates at 200 kV. High-resolution TEM (HRTEM) was carried out at 200 kV. The element mapping was obtained on an Tecnai F20 at 200 kV. X-ray photoelectron spectra (XPS) system was carried on a Thermo Fisher ESCALAB 250 with a monochromatic Al Kα X-ray source.

2.5. Electrochemical measurements

We used a CHI760e electrochemical workstation to test electrochemical properties at room temperature. In the experiment, the NF was used as the working electrode, and an Ag/AgCl (3 mol/L KCl) was utilized reference electrode and a carbon rod as the counter electrode. The electrocatalytic activity of catalysts for OER and HER were performed in 1 mol/L KOH (pH 14) solution. Before the test, high-purity argon was introduced to the electrode for 30 min. For HER performance, linear sweep voltammograms (LSV) were conducted at a scan rate of 5 mV/s. For OER performance, linear sweep voltammograms (LSV) were conducted at a scan rates of 2 mV/s. Electrochemical impedance spectroscopy (EIS) were employed in a frequency region of 0.01 Hz to 100 kHz. The potential values were calibrated to the reversible hydrogen electrode (RHE) according to the equation: $E_{RHE} = E_{Ag/AgCl} + 0.059\text{-}pH + 0.197$.

3. Result and discussion

In this study, the NiCo-LDH@Co_9S_8/NF was synthesized by a three-step hydrothermal method as illustrated in Fig. 1a. First, NF was used as the substrate, and the Co precursors grew on NF by a hydrothermal reaction. Next, the NF was put in Na_2S solution to form the Co_9S_8 nanowires arrays by an ion-exchange reaction. Finally, the Co_9S_8 nanowires was treated in the solution contains Ni^{2+} and Co^{2+} for forming NiCo-LDH, and Fig. S1 (online) shows the photograph of the four examples. The mass loading is about 1.8 mg/cm^2.

Fig. 1b showed the XRD patterns of Co_9S_8 and NiCo-LDH@Co_9S_8. In order to avoid the influence of the peak of metallic nickel, the catalyst was scraped off the NF before the test. The peaks located at 29.8°, 31.1°, 44.8°, 47.5°, 51.9°, 54.6° and 60.9° and was well matched to the (3 1 1), (2 2 2), (4 2 2), (5 1 1), (4 4 0), (5 3 1) and (5 3 3) planes of the Co_9S_8 (JCPDS No. 02-1459) [24]. The other peaks can be indexed to Ni_3S_2 (JCPDs No. 44-1418) [25], which came from the partial sulfidation of NF. In the pattern of Co_9S_8@-NiCo-LDH, the remaining peaks could attributed to (0 0 6), (0 1 2), (0 1 5) and (1 1 0) planes of NiCo LDH (JCPDS No. 40-0216) [26]. The above results suggested that the Co_9S_8 and NiCo LDH were successfully fabricated on the NF.

Fig. S2 (online) showed the Co precursor on NF, and Fig. 1c showed typical SEM image of Co_9S_8/NF: the Co_9S_8 nanowires grow on the surface of NF skeleton uniformly and the diameter of the nanowire was approximately 100 nm. Fig. 1d and e showed SEM images with different magnifications of the Co_9S_8@NiCo LDH/NF. Compared with Co_9S_8/NF, the surface of the nanowires became rough. Through careful observation, we found the ultrathin nanosheets grew on the surface of Co_9S_8 nanowire, which confirmed the formation of the Co_9S_8@NiCo LDH/NF 3D heterogeneous structure after the third hydrothermal treatment. The morphology and structure of the catalyst was further investigated with TEM and HRTEM. Fig. 2a showed the Co_9S_8 nanowires. The diameter of the nanowire was about 100 nm, which identical with SEM images. Fig. 2b showed the core-shell structure of Co_9S_8@NiCo-LDH. The nanosheets with the thickness less than 10 nm was coated on the surface of the nanowire homogeneously (Fig. S3 online). The HRTEM of Co_9S_8@NiCo-LDH/NF in Fig. 2c showed that the core phase has lattice spacings of 0.291 nm that attributed to the (3 1 1) plane of Co_9S_8 (JCPDs No. 02-1459) [27], and that the lattice fringes with interplane spacings of 0.219 and 0.251 nm in the shell (the thin nanosheet) can be attributed to (0 1 5) and (0 1 2) plane of NiCo LDH (JCPDS No. 40-0216) [28]. Fig. 2e displayed the energy-dispersive spectroscopy (EDS) elemental mapping analysis of the core-shell structure: the element Co was uniformly dispersed in the whole region, the Ni and O components were mainly dispersed in the shell region, and the S component was distributed in the core nanowire region. These results further demonstrated the Co_9S_8@NiCo LDH core-shell structure.

The detailed elemental valence states of NiCo-LDH@Co_9S_8/NF were investigated by XPS. Fig. 3a showed the full spectra of composites, in which four elements including Co, Ni, S and O were detected. Fig. 3b and c showed the spectra of Co 2p and Ni 2p. And both of them can be well fitted into two shakeup satellites (identified as Sat.) and two spin-orbit doublets. In the Co 2p spectrum, the peaks at binding energies of 780.0 and 795.8 eV were attributed to Co^{3+}, and the other located at 781.7 and 797.4 eV

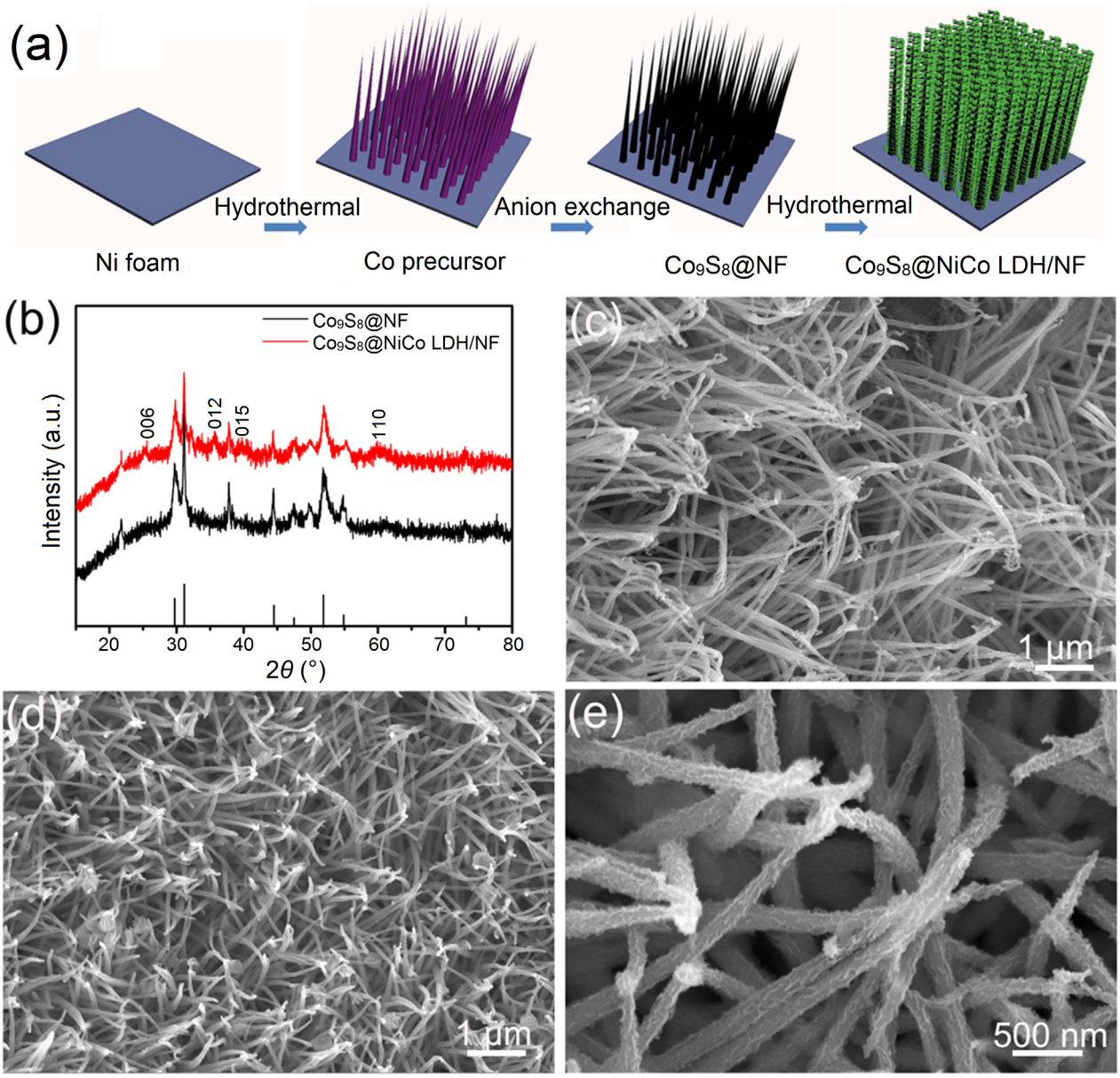

Fig. 1. (Color online) The synthesis procedure and the XRD and SEM characterizations. (a) Schematic illustration of the synthesis of Co_9S_8@NiCo LDH/NF; (b) XRD patterns of Co_9S_8@NiCo LDH and Co_9S_8 scrapped from NF; (c) SEM images of Co_9S_8 nanowires/NF; (d), (e) Co_9S_8@NiCo LDH/NF.

were attributed to Co^{2+} [29]. As to the Ni 2p spectrum, the Ni^{2+} peaks located at binding energies of 855.4 and 873.0 eV, the Ni^{3+} peaks located at 857.1 and 874.5 eV [30]. Fig. 4d showed the S 2p spectrum, it can be fitted into three peaks. One peak located at 168.5 eV can be assigned to the shakeup satellites, and the other two peaks at 163.0 and 161.3 eV were assigned to S $2P_{1/2}$ and S $2P_{3/2}$. Particularly, the peak at 161.3 eV corresponded to S^{2-} [31], and the other was ascribed to metal-sulfur bond. The above analysis indicated that the composites contained Co^{3+}, Co^{2+}, Ni^{3+}, Ni^{2+} cations and S^{2-} anion, which was consistent with recent reports [32,33]. And the analysis also confirmed the catalyst is composed by Co_9S_8 and NiCo-LDH.

The OER performance was investigated in a typical three-electrode system with 1 mol/L O_2-saturated KOH solution. For comparison, NiCo LDH/NF, Co_9S_8/NF and the bare NF was tested under the same condition. Fig. 4a presented polarization curves (with IR-compensation) of samples, from which we can see some anodic oxidation peaks located at overpotential from 1.2 to 1.4 V, and the peaks corresponded to the oxidation of Co^{2+} to Co^{3+} and Ni^{2+} to Ni^{3+} [34]. And the size of the oxidation peak depended on the quantity of element. The Co_9S_8@NiCo LDH/NF could afford the current density of 30 mA/cm^2 at an overpotential of 278 mV, which was lower than NiCo LDH/NF (331 mV), Co_9S_8/NF (310 mV) and bare NF (510 mV). Similarly, at a high current density, the heterogeneous structure exhibited the best performance, which only needs 330 mV to reach current density at 100 mA/cm^2. The overpotential was lower than that of recent reported studies (Table S1 online). Tafel slope is an important means to evaluate electrocatalysts kinetics, and it can be obtained from the Tafel equation, $\eta = b\log|j| + a$ (where η represents the overpotential, b represents the Tafel slope and j represents the current density) [35]. Fig. 4b exhibited the tafel slope of OER, the slope of Co_9S_8@-NiCo LDH/NF was 83 mV/dec, lower than Co_9S_8/NF (100 mV/dec), NiCo LDH (117 mV/dec), NF (125 mV/dec). The combination of Co_9S_8/NF and NiCo LDH can largely increase the OER performance according to the above results. EIS is another tool to understand

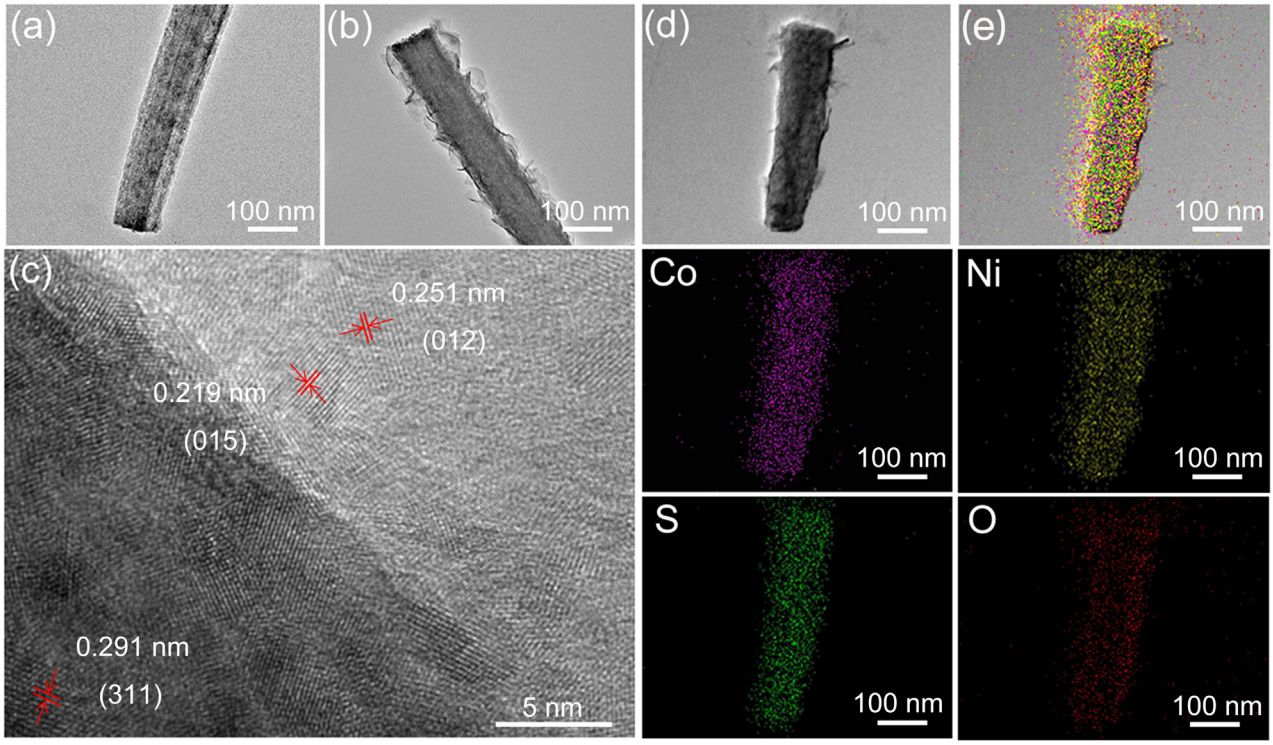

Fig. 2. (Color online) TEM images. (a) Co_9S_8 nanowires scrapped from NF; (b) Co_9S_8@NiCo LDH scrapped from NF. (c) HRTEM image of Co_9S_8@NiCo LDH; (d, e) EDS mapping of Co_9S_8@NiCo LDH.

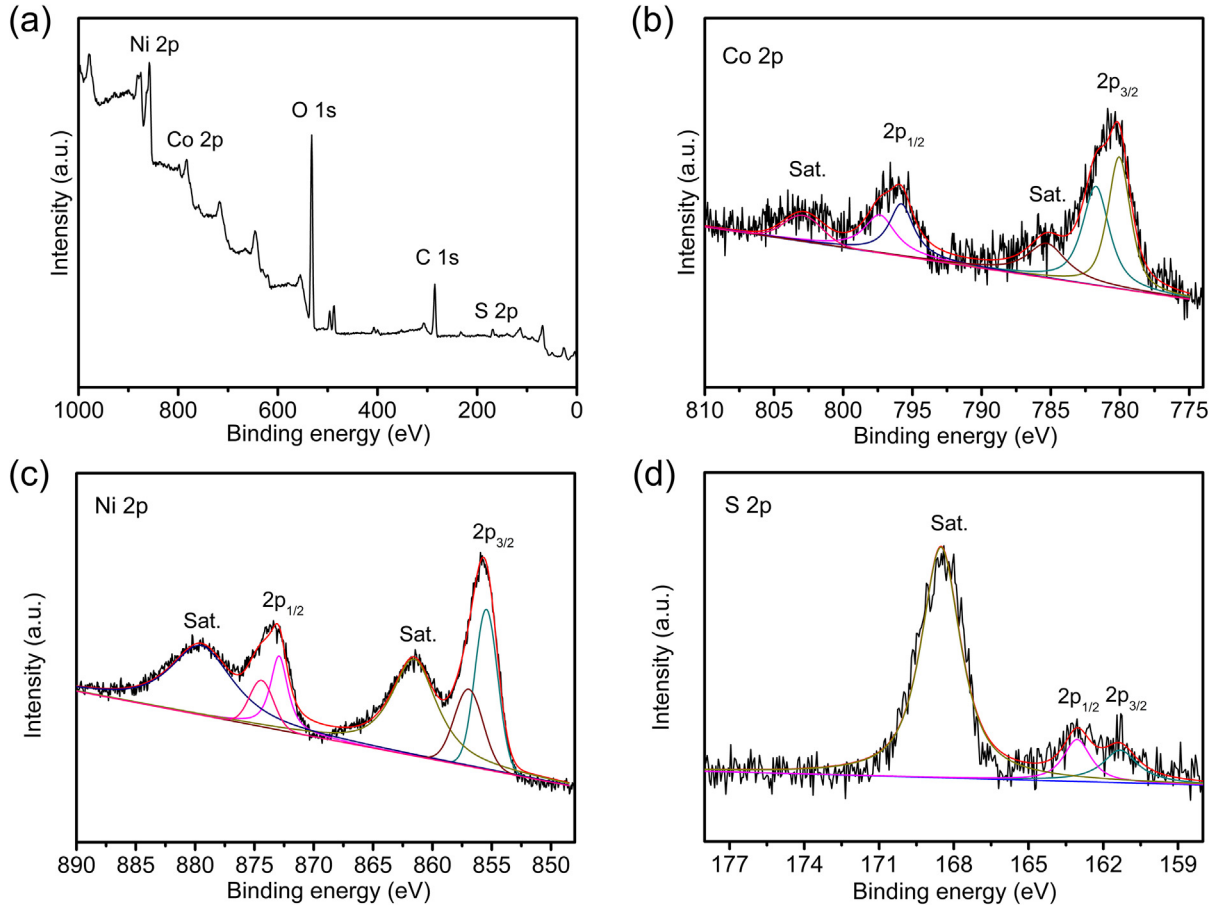

Fig. 3. (Color online) XPS analysis. (a) XPS full spectrum of Co_9S_8@NiCo LDH; high-resolution spectrum of (b) Co 2p spectra, (c) Ni 2p spectra, and (d) S 2p spectra.

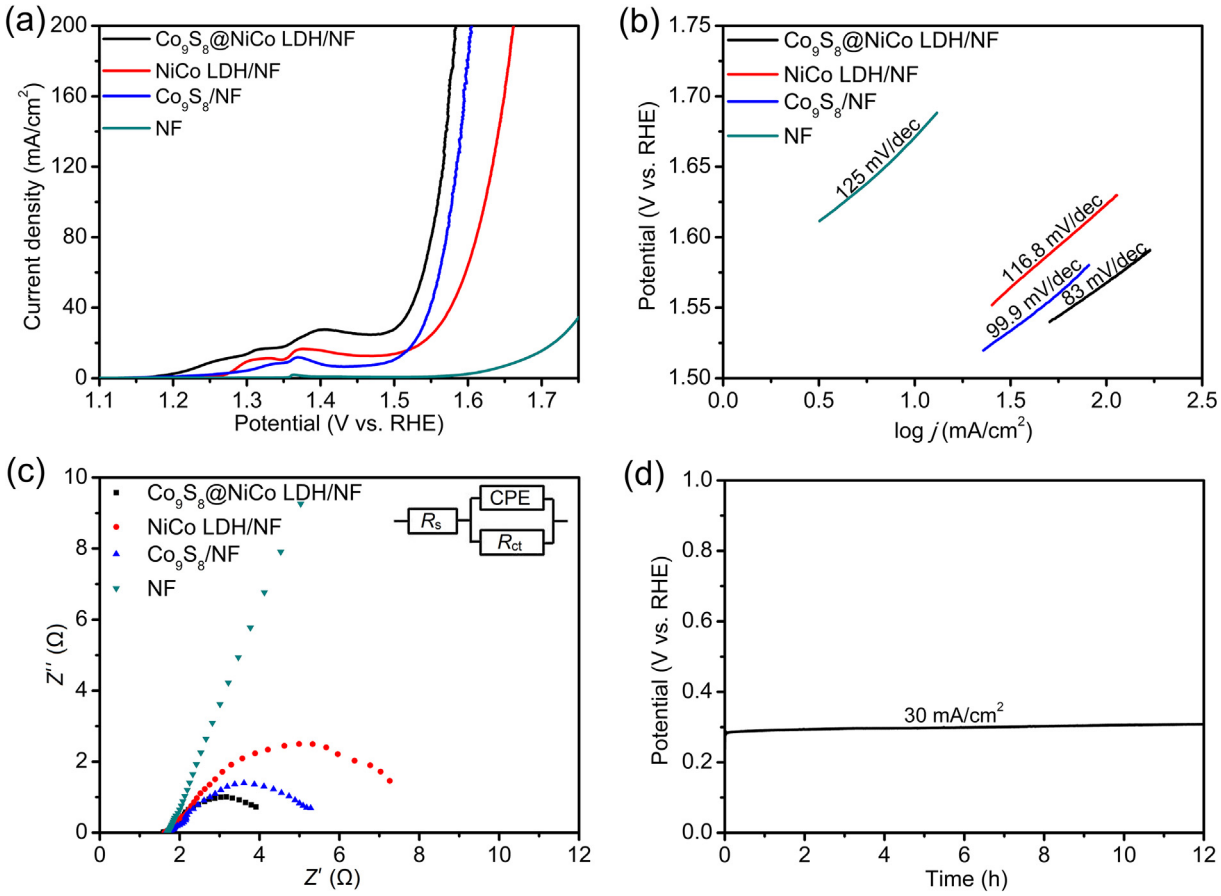

Fig. 4. (Color online) OER performance. (a) LSV curves of Co_9S_8@NiCo LDH/NF, NiCo LDH/NF, Co_9S_8/NF and NF; (b) Tafel plots of Co_9S_8@NiCo LDH/NF, NiCo LDH/NF, Co_9S_8/NF and NF; (c) Nyquist plots of the Co_9S_8@NiCo LDH/NF, NiCo LDH/NF, Co_9S_8/NF and NF electrodes (equivalent circuit in inset); (d) chronopotentiometry durability test of Co_9S_8@NiCo LDH/NF.

the electrode kinetics. The corresponding Nyquist plots were shown in Fig. 4c, and the upper right corner displayed the equivalent circuit. R_s means the solution resistance and R_{ct} means the charge transfer resistance. The R_s is almost same for different catalysts because of the same electrolyte (1 mol/L KOH). Lower R_{ct} value reflected a fast charge transfer process and a fast reaction rate [36]. The Nyquist semicircular diameter of the Co_9S_8@NiCo LDH/NF is smallest among the four samples, which indicates the heterogeneous structure has a smaller reaction resistance and fast faradaic process. On one hand, the excellent performance should be attributed to high specific surface area and numerous active sites provide by the well-arranged Co_9S_8@NiCo LDH nanoarrays. On the other hand, the Co_9S_8@NiCo LDH arrays directly grown NF benefit to electrons transfer and gas release. The stability test was carried at a constant current density of 30 mA/cm^2. As shown in Fig. 4d, we can only see a slight increase in overpotential after 12 h.

The HER performance was investigated in a typical three-electrode system in 1 mol/L H_2-saturated KOH solution. The other three materials were also tested. Fig. 5a showed the polarization curves, and Co_9S_8@NiCo LDH/NF displayed the best HER performance, which required only 168 mV to achieve 10 mA/cm^2, obviously smaller than that of NiCo LDH/NF (η_{10} = 234 mV), Co_9S_8/NF (η_{10} = 226 mV) and bare NF (η_{10} = 287 mV), better than the recently reported non-noble catalysts, as shown in Table S2 (online). It required a low overpotential of 276 mV to achieve the current density of 100 mA/cm^2. The difference toward HER performance can be reflected by the tafel plots, the tafel slope of the Co_9S_8@NiCo LDH/NF, NiCo LDH/NF, Co_9S_8/NF and bare NF is 103, 126, 123 and 153 mV/dec. Fig. 5c showed the Nyquist plot and the corresponding equivalent circuit, the value of Co_9S_8@NiCo-LDH/NF was about 10.8 Ω, which was smaller than Co_9S_8/NF (15.7 Ω), NiCo LDH/NF (12.03 Ω) and NF (32.5 Ω), suggesting fast charge transfer process during reactions. Furthermore, we examined the long-term stability of Co_9S_8@NiCo LDH/NF, as shown in Fig. 5d, and the overpotential remained basically unchanged after 12 h test at a constant current density of 10 mA/cm^2. The above results revealed the excellent performance of Co_9S_8@NiCo LDH/NF towards HER.

The electrochemical active surface area (ECSA) represent the density of active sites on catalyst surface, so we could estimate it through the electrochemical double-layer capacitance (C_{dl}) [18]. We carried out CV tests in the non-faradaic area (0.66–0.76 V vs. RHE) to obtain the C_{dl} in the different scan rate (10, 20, 30, 40, 50 mV/s). Fig. 6a showed the CV curves of Co_9S_8@NiCo LDH/NF, Co_9S_8/NF and NiCo LDH/NF. Fig. S4a and b (online) showed the CV curves of the Co_9S_8/NF and NiCo LDH/NF, the anodic (i_a) capacitive current and cathodic (i_c) capacitive current at 0.72 V were shown in Fig. S5 (online). The calculated C_{dl} values in Fig. 6d are 64, 44.5 and 25 mF/cm^2 for Co_9S_8@NiCo LDH/NF, Co_9S_8/NF and NiCo LDH/NF respectively. These values indicated the Co_9S_8@NiCo LDH/NF possess the largest ECSA, which came from the rational combination of the Co_9S_8 nanowires with NiCo LDH nanosheets. The large ESCA is responsible for the excellent HER and OER activities.

Based on the above discussions, the 3D core-shell structure of Co_9S_8@NiCo LDH showed the outstanding performance toward

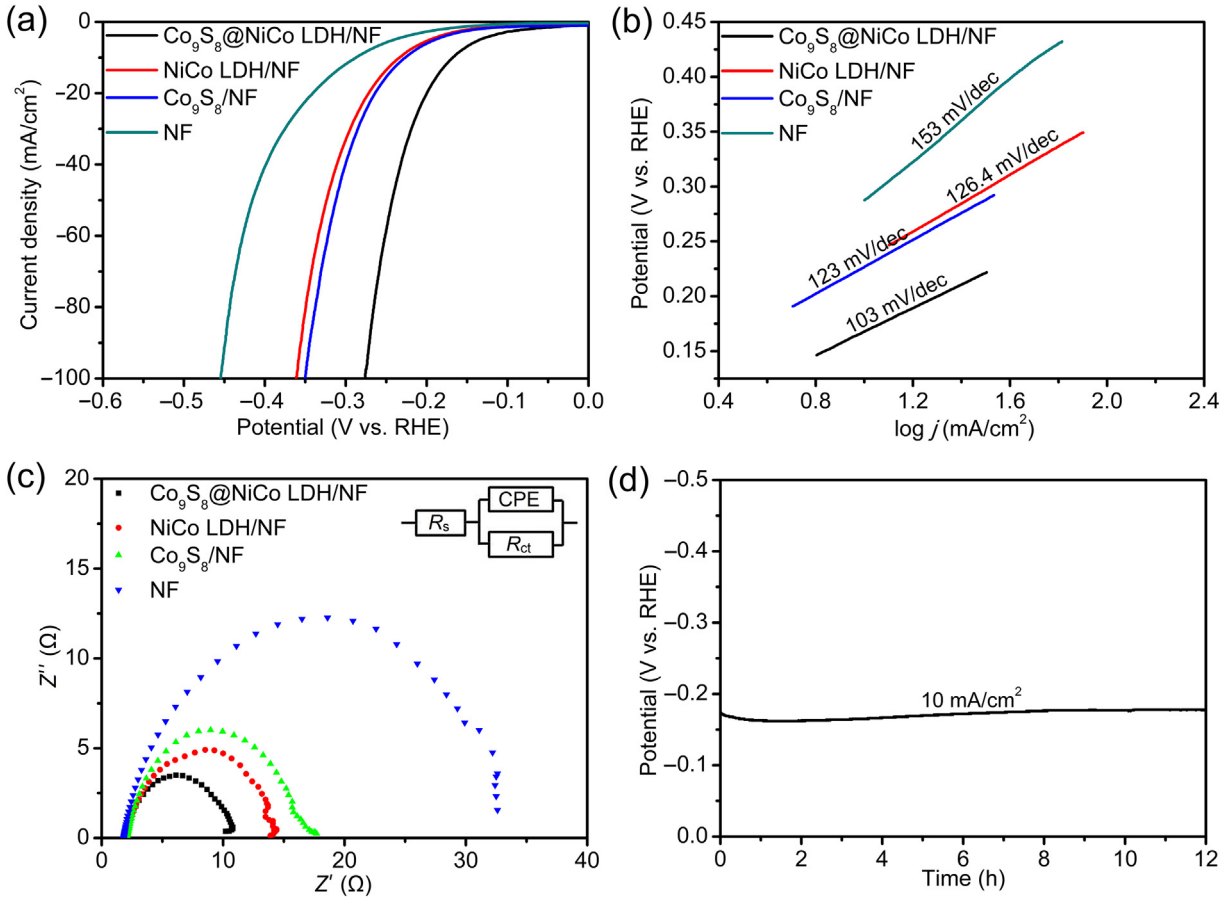

Fig. 5. (Color online) HER performance. (a) LSV curves of Co_9S_8@NiCo LDH/NF, NiCo LDH/NF, Co_9S_8/NF and NF; (b) Tafel plots of Co_9S_8@NiCo LDH/NF, NiCo LDH/NF, Co_9S_8/NF and NF; (c) Nyquist plots of the Co_9S_8@NiCo LDH/NF, NiCo LDH/NF, Co_9S_8/NF and NF electrodes (equivalent circuit in inset); (d) chronopotentiometry durability test of Co_9S_8@NiCo LDH/NF.

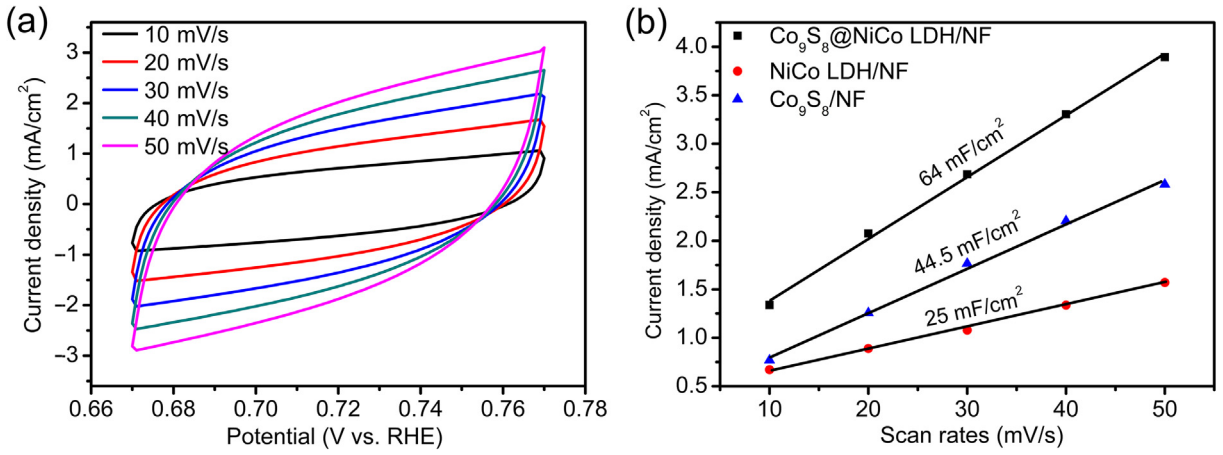

Fig. 6. (Color online) C_{dl} calculations. (a) Cyclic voltammograms for Co_9S_8@NiCo LDH/NF; (b) double layer capacitance of Co_9S_8@NiCo LDH/NF, Co_9S_8/NF and NiCo LDH/NF.

OER and HER. Therefore, a water-splitting electrolyzer system was used to investigate the overall water splitting performance, the Co_9S_8@NiCo LDH/NF served as both anode and cathode in 1 mol/L KOH solution. As displayed in Fig. 7a, the electrode required 1.63 V to reach the current density of 10 mA/cm^2, which demonstrated excellent catalytic activity. We can see bubbles generated on the surface of the electrode clearly during the electrolysis process. Table S3 (online) showed the performance comparison to reach the current density of 10 mA/cm^2 with other recently reported non-noble bifunctional catalysts. The data pointed out that the Co_9S_8@NiCo LDH/NF has better overall water splitting performance. The stability test was carried out under the constant current density of 10 mA/cm^2 and provided in Fig. 7b, Only slight change (<0.6%) in potential was observed over 12 h, exhibiting the superior long-term stability.

SEM and XRD characterizations were applied to analyze structure and composition evolution of the Co_9S_8@NiCo LDH/NF after overall water splitting test. Fig. S6a and b (online) represent

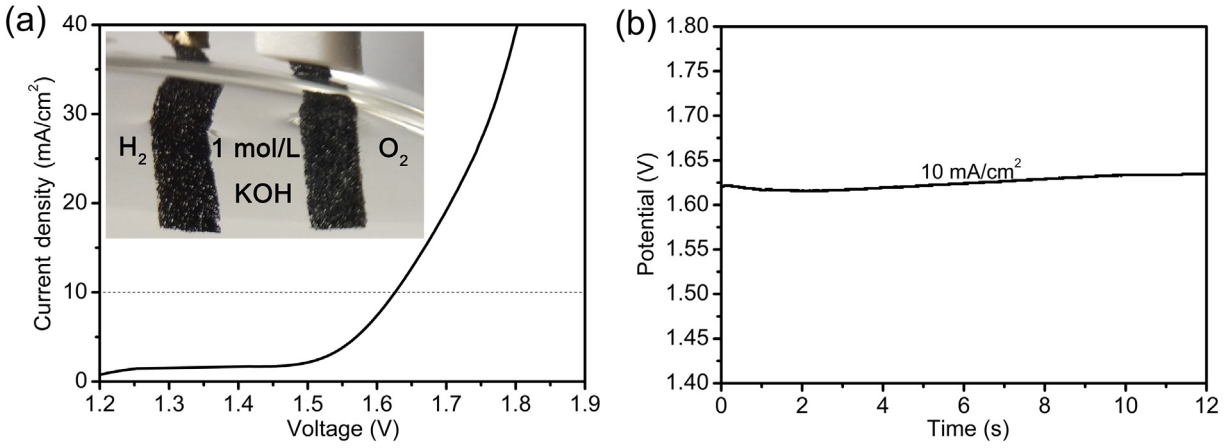

Fig. 7. (Color online) Overall water splitting performance. (a) Polarization curves for overall water splitting with Co_9S_8@NiCo LDH/NF electrode as both the anode and cathode at scan rate of 5 mV/s; (b) Chronopotentiometry durability test of Co_9S_8@NiCo LDH/NF at a constant current density of 10 mA/cm^2 over 12 h in a two-electrode configuration.

the SEM images of Co_9S_8@NiCo LDH/NF after test, and the structure collapsed slightly and some particles appeared on the surface after OER (shown in Fig. S6a online). There is almost no change in structure after HER (shown in Fig. S6b online). The results demonstrated that the mechanical robustness of the catalyst. Fig. S6c and d (online) showed the corresponding XRD pattern after OER and HER. The XRD pattern after HER remained unchanged, but we found the peaks of NiCo LDH disappeared after OER test, and the emerging peaks can be attributed to NiOOH and CoOOH, and they were transformed from NiCo LDH. The results suggested that the NiOOH and CoOOH are the active composition for OER, which is consistent with relevant studies [37].

4. Conclusion

In summary, we have successfully fabricated a novel 3D Co_9S_8 nanowires@NiCo LDH nanosheets grown on NF by a three-step hydrothermal approach. The conductivity was greatly improved by using NF as the substrate. The active components of catalyst grow directly on the nickel foam without using polymeric binders, promising strong durability under high current density and better catalytic performance. The open framework enables efficient mass transfer, and benefit to the generation and removal of gas bubbles. The synergetic effect of NiCo LDH, Co_9S_8 and NF optimizes the catalytic activity. All these factors lead to the remarkable catalytic activities toward HER and OER, and make Co_9S_8@NiCo LDH/NF an excellent bifunctional catalyst for water splitting.

Conflict of interest

The authors declare that they have no conflict of interest.

Acknowledgments

This work was supported by the National Natural Science Foundation of China (21571012).

Appendix A. Supplementary data

Supplementary data to this article can be found online at https://doi.org/10.1016/j.scib.2019.01.006.

References

[1] Dresselhaus MS, Thomas IL. Alternative energy technologies. Nature 2001;414:332–7.
[2] Morales-Guio CG, Mayer MT, Yella A, et al. An optically transparent iron nickel oxide catalyst for solar water splitting. J Am Chem Soc 2015;137:9927–36.
[3] Liu X, Cui S, Sun Z. Robust and highly active copper-based electrocatalyst for hydrogen production at low overpotential in neutral water. Chem Commun 2015;51:12954–7.
[4] Xiao P, Sk MA, Thia L, et al. Molybdenum phosphide as an efficient electrocatalyst for the hydrogen evolution reaction. Energy Environ Sci 2014;7:2624–9.
[5] Zheng Y, Jiao Y, Jaroniec M, et al. Advancing the electrochemistry of the hydrogen-evolution reaction through combining experiment and theory. Angew Chem Int Ed 2015;54:52–65.
[6] Lee Y, Suntivich J, May KJ, et al. Synthesis and activities of rutile IrO_2 and RuO_2 nanoparticles for oxygen evolution in acid and alkaline solutions. J Phys Chem Lett 2012;3:399–404.
[7] Sato J, Saito N, Yamada Y, et al. RuO_2-loaded β-Ge_3N_4 as a non-oxide photocatalyst for overall water splitting. J Am Chem Soc 2015;127:150–1.
[8] Niu S, Jiang WJ, Tang T, et al. Facile and scalable synthesis of robust $Ni(OH)_2$ nanoplate arrays on NiAl foil as hierarchical active scaffold for highly efficient overall water splitting. Adv Sci 2017;4:1700084–89.
[9] Ren JT, Yuan GG, Weng CC, et al. Uniquely integrated Fe-doped $Ni(OH)_2$ nanosheets for highly efficient oxygen and hydrogen evolution reactions. Nanoscale 2018;10:10620–8.
[10] Wu H, Sun W, Shen J, et al. Role of flower-like ultrathin Co_3O_4 nanosheets in water splitting and non-aqueous Li-O_2 batteries. Nanoscale 2018;10:1021–31.
[11] Chen Z, Zhao H, Zhang J, et al. IrNi nanoparticle-decorated flower-shaped $NiCo_2O_4$ nanostructures:controllable synthesis and enhanced electrochemical activity for oxygen evolution reaction. Sci China Mater 2017;60:119–30.
[12] Zhang X, Gu W, Wang E. Self-supported ternary $Co_{0.5}Mn_{0.5}P$/carbon cloth (CC) as a high-performance hydrogen evolution electrocatalyst. Nano Res 2017;10:1001–9.
[13] Su J, Zhou J, Wang L, et al. Synthesis and application of transition metal phosphides as electrocatalyst for water splitting. Sci Bull 2017;62:633–44.
[14] Shengjie P, Linlin L, Xiaopeng H, et al. Cobalt sulfide nanosheet/graphene/carbon nanotube nanocomposites as flexible electrodes for hydrogen evolution. Angew Chem Int Ed 2015;126:12802–7.
[15] Lu S, Zhong Z. Electrocatalysts for hydrogen oxidation and evolution reactions. Sci China Mater 2016;59:1–22.
[16] Zhou H, Wang Y, He R, et al. One-step synthesis of self-supported porous $NiSe_2$/Ni hybrid foam: an efficient 3D electrode for hydrogen evolution reaction. Nano Energy 2016;20:29–36.
[17] Swesi AT, Masud J, Liyanage WPR, et al. Textured $NiSe_2$ film: bifunctional electrocatalyst for full water splitting at remarkably low overpotential with high energy efficiency. Sci Rep 2017;10:1–11.
[18] Chen L, Zhang J, Ren X, et al. A $Ni(OH)_2$-CoS_2 hybrid nanowire array: a superior non-noble-metal catalyst toward the hydrogen evolution reaction in alkaline media. Nanoscale 2017;9:16632–7.
[19] Xu H, Wang B, Shan C, et al. Ce-doped NiFe-layered double hydroxide ultrathin nanosheets/nanocarbon hierarchical nanocomposite as an efficient oxygen evolution catalyst. ACS Appl Mater Interfaces 2018;10:6336–45.
[20] Wang C, Tian B, Mei W, et al. Revelation of its excellent intrinsic activity of MoS_2|NiS|MoO_3 nanowire for hydrogen evolution reaction in alkaline medium. ACS Appl Mater Interfaces 2017;9:7084–90.
[21] Yao S, Zhang X, Zhou W, et al. Atomic-layered Au clusters on α-MoC as catalysts for the low-temperature water-gas shift reaction. Science 2017;357:389–93.

[22] Ren Z, Du S, Bai X, et al. In-situ structure reconstitution of $NiCo_2P_x$ for enhanced electrochemical water oxidation. Sci Bull 2017;62:1510–8.
[23] Zhu H, Jiang R, Chen X, et al. 3D nickel-cobalt diselenide nanonetwork for highly efficient oxygen evolution. Sci Bull 2017;62:1373–9.
[24] Yang Q, Liu L, Xiao L, Zhang L, et al. Co_9S_8@N, S-codoped carbon core-shell structured nanowires: constructing fluffy surface for high-density active sites. J Mater Chem A 2018;7:14752–60.
[25] Zhou W, Wu XJ, Cao X, et al. Ni_3S_2 nanorods/Ni foam composite electrode with low overpotential for electrocatalytic oxygen evolution. Energy Environ Sci 2013;6:2921–4.
[26] Yu C, Liu Z, Han X, et al. NiCo-layered double hydroxides vertically assembled on carbon fiber papers as binder-free high-active electrocatalysts for water oxidation. Carbon 2016;110:1–7.
[27] Feng L, Fan M, Wu Y, et al. Metallic Co_9S_8 nanosheets grown on carbon cloth as efficient binder-free electrocatalysts for the hydrogen evolution reaction in neutral media. J Mater Chem A 2016;4:6860–7.
[28] Zhang H, Tong Y, Xu J, et al. In situ antisolvent approach to hydrangea-like HCo_3O_4-NC@CoNi-LDH core@shell superstructures for highly efficient water electrolysis. Chemistry 2017;24:400–8.
[29] Jiang J, Zhang A, Li L, et al. Nickel-cobalt layered double hydroxide nanosheets as high-performance electrocatalyst for oxygen evolution reaction. J Power Sources 2015;278:445–51.
[30] Wang T, Zhang S, Yan X, et al. 2-Methylimidazole-derived Ni-Co layered double hydroxide nanosheets as high rate capability and high energy density storage material in hybrid supercapacitors. ACS Appl Mater Interfaces 2017;9:15510–24.
[31] Wang F, Zhu Y, Tian W, et al. Co-doped Ni_3S_2@CNTs array anchored on graphite foam with hierarchical conductive network for high-performance supercapacitor and hydrogen evolution electrode. J Mater Chem A 2018;6:10490–6.
[32] Wang S, Dou S, Tao L, et al. Etched and doped Co_9S_8/graphene hybrid for oxygen electrocatalysis. Energy Envir Sci 2016;9:1320–6.
[33] Liu Y, Teng X, Mi Y, et al. A new architecture design of Ni-Co LDH-based pseudocapacitors. J Mater Chem A 2017;5:24407–15.
[34] Wu J, Ren Z, Du S, et al. A highly active oxygen evolution electrocatalyst: ultrathin CoNi double hydroxide/CoO nanosheets synthesized interface-directed assembly. Nano Res 2016;9:713–25.
[35] Jing G, Long K, Erjie K, et al. Precious-metal-free Co-Fe-O/rGO synergetic electrocatalysts for oxygen evolution reaction by a facile hydrothermal route. ChemSusChem 2018;5:659–64.
[36] Wang J, Zhong H, Qin Y, et al. An efficient three-dimensional oxygen evolution electrode. Angew Chem Int Ed 2013;52:5248–53.
[37] Yan Z, Sun H, Chen X, et al. Anion insertion enhanced electrodeposition of robust metal hydroxide/oxide electrodes for oxygen evolution. Nat Commun 2018;9:2373–86.

Jingan Yan joined the School of Chemical Engineering, Beijng University of Chemiacl Technology to study for his master's degree in 2016. His research direction is electrolytic water splitting. He focuses on design and synthesis the bifunctional electrocatalysts that composed by transition metal compound, therefore, reduce the cost of hydrogen produced by water electrolysis.

Xin Liang is an associate professor at Beijing University of Chemical Technology. She received her Ph.D. degree from the Department of Chemistry, Tsinghua University in 2009. She worked in the University of California, Santa Barbara from 2013−2014 as a research fellow. Her research interests include design, synthesis and characterization of functional catalytic materials towards industrial and energy catalysis, such as hydrodesulfurization, hydrogenations and electrocatalysis.